Heliyon 8 (2022) e12360

Contents lists available at ScienceDirect

Heliyon

journal homepage: www.cell.com/heliyon

Research article

# Simulation of transient heat transfer during forced convection cooling of cocoyam *(Colocasia Esculenta* (L.) Schott*)* tubers

John Ndisya [a,b,c,*], Ayub Gitau [b], Franz Roman [a], Duncan Mbuge [b], Barbara Sturm [a,d,e,**], Oliver Hensel [a]

[a] Department of Agricultural & Biosystems Engineering, Faculty of Organic Agricultural Sciences, University of Kassel, Nordbahnhof str. 1a, 37213 Witzenhausen, Germany
[b] Department of Environmental & Biosystems Engineering, School of Engineering, University of Nairobi, P.O. Box 30197-00100, Nairobi, Kenya
[c] Department of Agricultural & Biosystems Engineering, School of Engineering & Technology, Kenyatta University, P.O. Box 43844 – 00100, Nairobi, Kenya
[d] Leibniz Institute for Agricultural Engineering and Bioeconomy (ATB), Max-Eyth Allee 100, 14469 Potsdam, Germany
[e] Albrecht Daniel Thaer-Institute of Agricultural and Horticultural Sciences, Humboldt Universität zu Berlin, Hinter der Reinhardtstr. 6–8, 10115 Berlin, Germany

ARTICLE INFO

*Keywords:*
Field heat removal
Forced convection precooling
Transient heat transfer
Postharvest storage

ABSTRACT

In this study, a prediction model based on transient heat transfer was modified and validated using experimental data. The time required to cool tubers from field temperature of 30 ± 2 °C to the target storage temperature of 12 ± 0.2 °C was predicted directly from the model. Moreover, total cooling time ranged from 127.8 – 154.2 min for small tubers and 190.8–262.2 min for large tubers while the field heat removed ranged from 9.61 – 10.17 kJ for small tubers and 24.78–31.90 kJ for large tubers between the extremes of the air velocity. Tuber orientation to airflow neither influenced the heat transfer coefficients and Biot numbers nor the cooling time and amount of field heat removed. The results from this study could be applied in the design and optimisation of forced convection cooling systems to precool tubers immediately after harvest and for extended duration storage.

## 1. Introduction

*Cocoyam (Colocasia esculenta* (L.) Schott*)* is a nutrient-dense tuber crop grown in tropical and subtropical regions of the world for food (Fern, 2018). Its uptake and commercialisation are however hindered by poor storability in the fresh form (Ndisya et al., 2020). Immediately after harvesting, the tubers undergo rapid rot or sprouting when stored under ambient conditions (Lewu et al., 2010; Opata and Ogbonna, 2015). As compared to other root and tuber crops such as sweet potato, potato and cassava, limited post-harvest technologies and techniques have been developed for cocoyam (Lewu et al., 2010). Recent studies on the preservation of cocoyam tubers have mainly focused on the production of dried products and their derivatives (Aboubakar et al., 2009; Afolabi et al., 2015; Kumar et al., 2017; M Alcantara, 2013; Ndisya et al., 2020; Zhang et al., 2017). Traditionally, cocoyam tubers are either harvested for immediate consumption or left buried in the farm as a way of storage until needed (Opara, 2003). Moreover, infield storage not only ties-up land that could be used for a new crop but also affects the quality of the tubers. Infield storage beyond the optimal maturity age is associated with tuber rot (Modi, 2007; Wang and Higa, 1983) and a decline in the quality of starch (Himeda et al., 2012). Documented improved storage methods include storage in traditional low-cost structures and pits (Opara, 1999), ventilated stores (Thompson, 2003) and refrigerated storage (Opara, 2003). These methods have registered widely varying degrees of success chiefly due to varying simplicity, performance, and affordability. But none of these achieves the same level of success as refrigeration (Opara, 1999).

Convective cooling is a technique commonly applied to improve the storage conditions of agricultural products in place of the comparatively expensive refrigeration methods (Basediya et al., 2013). Cooling preserves the natural quality of products by suppressing physiological, biochemical, and microbiological processes (Dehghannya et al., 2010). The development of a cooling solution requires the knowledge of how a product's thermophysical properties interact with the temperature, velocity, and relative humidity of the cooling medium (Korese et al., 2017; van Gogh et al., 2017). Previous studies have explored the interrelationship between these factors for agricultural products including grapes (Dincer, 1995), oranges (Elansari and Mostafa, 2020), sweet potatoes (Korese et al., 2017), tomato (R. Kumar et al., 2008), meat and poultry (Marcotte et al., 2008) among other products. Various techniques based

* Corresponding author.
** Corresponding author.
*E-mail addresses:* jndisyas@gmail.com (J. Ndisya), director@atb-potsdam.de (B. Sturm).

https://doi.org/10.1016/j.heliyon.2022.e12360
Received 19 June 2022; Received in revised form 7 November 2022; Accepted 7 December 2022

on the fundamental principles of heat and mass transfer have been applied to study and model this relationship. Some of these studies are empirical (Dincer, 1997; Krokida et al., 2002). However, the experiments involved are resource-costly and the results can only be applied for the specific products they have been developed for and are therefore less versatile (Korese et al., 2017; Wang et al., 2001; Zou, Opara and McKibbin, 2006a). Computer-based modelling has simplified the analysis and optimization of physical parameters to improve heat and mass transfer and aid in the design of appropriate packaging (Zou, Opara and McKibbin, 2006b). However, the computational methods involved often require the utilization of complex mathematical principles and propriety software (Davey, 2015). Moreover, Romdhana et al.(2016) argued that the available proprietary simulation programmes are often confined to steady-state simulations because the solution of equations for transient heat and mass transfer requires spatiotemporal discretization and therefore significant computing power for solution stability and convergence. To achieve wider adoption in a practical setting particularly in rural farms where access to advanced computational resources is limited, simpler and computationally-convenient mathematical models which adequately estimate the heat transfer behaviour are needed (Davey, 2015; Korese et al., 2017).

When the spatial variation of temperature is negligible and the state change is assumed to be purely temporal, lumped system analysis can be applied to study transient heat transfer (Çengel and Ghajar, 2015). In this case, the Biot number (Bi) is less than 0.1 and the material exhibits negligible internal resistance to heat transfer (Phongikaroon and Calabrese, 2005). Tegenaw et al. (2019) compared the results of simulations from CFD and lumped system models in simulating heat transfer. The lumped system model results matched those from the CFD model but required lesser computational effort. Lumped system analysis has been successfully applied to study heat transfer in various products including figs (Dincer, 1994), grapes (Dincer, 1995), fish (Davey, 2015) and sweet potatoes (Korese et al., 2017). Nevertheless, the internal resistance to heat transfer for most thermal systems are often significant and therefore, the simple lumped system analysis approach is seldom applicable in such cases (Ranmode et al., 2019). This is because the spatial variation of temperature becomes significant and the Biot number increases beyond 0.1 (Çengel and Ghajar, 2015). However, recent studies have successfully extended the validity of lumped system analysis to cases where $Bi > 0.1$. Xu et al. (2012) and Jian et al. (2015) derived and tested new equations for calculating effective heat transfer coefficients for simple infinite geometries of relevance to thermal energy storage applications for use in scenarios where $Bi > 0.1$. The results obtained with the utilisation of effective heat transfer coefficients with lumped systems analysis were in good agreement with experimental data and analytical solutions. When the effective heat transfer coefficients and the resulting Biot numbers are used in the place of the heat transfer coefficients and Biot numbers in the lumped models, the heat transfer problem can be solved directly using the lumped system analysis method (Xu et al., 2012). In this case, the characteristic dimension utilised to compute the effective Biot number and the Fourier number for the cylinder geometry is half the radius of the cylinder rather than the full radius as typically used in the exact analytical solution (Ranmode et al., 2019; Xu et al., 2012). Lumped system models can be used to study the temperature distribution and heat transfer in one-dimensional heat transfer problems associated with infinite geometries such as large slabs and long cylinders. However, when the geometries can no longer be considered to be infinite, heat transfer is multidimensional and the governing equations can be constructed using a product solution approach (Çengel and Ghajar, 2015; Christensen and Adler-Nissen, 2015).

The objective of this study was to investigate the influence of air velocity, tuber size and tuber orientation on airflow on the cooling behaviour of whole cocoyam tubers. Çengel and Ghajar (2015) proposed a product solution approach based on the fundamental transient heat transfer analysis to solve heat transfer problems in multidimensional geometries. The second objective of this study was to modify the modelling approach by Çengel and Ghajar (2015) and to investigate its applicability in predicting the cooling time required to remove field heat from cocoyam tubers. The changes introduced included the estimation of thermophysical properties of the cocoyam tubers using food component models developed by Choi and Okos (1986) and the introduction of an effective heat transfer coefficient to the Biot number formulae following Xu et al. (2012). The results from the model were validated by comparing model predictions and experimental data. Method comparison techniques including the Symmetric Median Absolute Percentage Error (Morley et al., 2018), Huber regression slope and intercept (Huber, 2004), Bland-Altman plots (Bland and Altman, 1999) and the Concordance Correlation Coefficient (Barnhart et al., 2007) were utilised.

## 2. Materials and methods

### 2.1. Materials

This study utilised cocoyam (*Colocasia esculenta* (L.) *Schott)* tubers harvested at maturity and carefully sorted by hand to select tubers without visible defects. The soil left on the tuber surfaces during harvesting was gently removed using a soft brush. The tubers were then trimmed at both ends to remove dried material formed on the previous scar at the bottom end and at the petiole base to remove the foliage. The tubers were then cured by placing them in open sunlight for about 8 h until the wounded surfaces dried out.

### 2.2. Experimental design, apparatus, and material properties

#### 2.2.1. Experimental design

Table 1 provides the experimental design parameters and settings utilised in this study. Forced convection cooling experiments were conducted at three levels of air velocity, two levels of tuber size and two levels of tuber orientation to the airflow of cooling air. Cocoyam tubers were cooled in air at 90 ± 2% relative humidity and 10 ± 0.2 °C temperature from an initial temperature of 30 ± 2 °C at the core and 28 ± 2 °C under the skin of the tubers to a uniform final temperature of 12 ± 0.2 °C. A replicated and completely randomised full factorial experimental design was created in the Design-Expert software version 11 (Stat-Ease Inc., Minneapolis, United States) and utilised to conduct experiments.

#### 2.2.2. Experimental apparatus

The experimental test apparatus utilised included a VCL 400 climate chamber (Vötsch Industrietechnik GmBH, Reiskirchen-Lindenstruth, Germany) with a temperature range of - 40 to +180 ± 0.5 °C and relative humidity range of 10–98 ± 3%. To achieve control over air velocity, a test box fully insulated with glass wool was utilised. The test box was instrumented with an EBM-Papst 3218JH4 variable speed fan (EBM-Papst Inc., St. Georgen, Germany), PHYWE-07475 voltage controller (PHYWE Systeme GmbH, Göttingen, Germany), air inlet duct and plenum. The data collection mechanism consisted of Pt-1000 RTD sensors (Therma Thermofühler GmbH, Lindlar Germany) linked to an Agilent Keysight 34970A multi-channel data logger (Keysight Technologies, California, USA). For this study, the temperature sensors were placed approximately at the core of the tubers and about 2 mm below the skin of the tubers. The air velocity was measured at the sample location using a TA-5 thermal anemometer (Airflow Lufttechnik GmbH, Rheinbach, Germany). The complete experimental set-up is presented in Figure 1.

#### 2.2.3. Material properties

The thermophysical properties of the cocoyam material were estimated from the models formulated by Choi and Okos (1986) using properties of air at standard atmospheric pressure (i.e., 101.325 kPa) and 10 °C air temperature (Rohsenow et al., 1998). The models provide a method to estimate properties as a function of major food constituents and temperature. The ratios of the constituents in cocoyam tubers are

**Table 1.** Experimental design parameters.

| Design parameter | Units | Settings |
|---|---|---|
| Air velocity | m/s | 0.5, 0.7, 0.9 |
| Tuber size | [−] | **Large**: m = 466.98 ± 95 g, l = 115.25 ± 23 mm, d = 72.08 ± 6 mm **Small**: m = 173.42 ± 30 g, l = 83.21 ± 11 mm, d = 51.44 ± 4 mm |
| Tuber orientation to airflow | [−] | Along, Across |

provided as supplementary data while the material properties are provided in Table 2.

### 2.3. Mathematical framework

#### 2.3.1. Key assumptions

The mathematical models for the solution of transient heat transfer equations for whole cocoyam tubers are based on the following assumptions: -

- The properties of the cooling air remain constant throughout the experiments;
- The range of air velocity (i.e., 0.5, 0.7, 0.9 m $s^{-1}$) is sufficiently subsonic (i.e., less than Mach 0.3) to guarantee incompressibility (Kundu et al., 2012);
- The flow domain wall condition is perfectly insulated to prevent thermal gains and losses;
- The thermophysical properties of cocoyam tubers can be adequately estimated using the models by Choi and Okos (1986);
- Each cocoyam tuber can be idealised as a short cylinder with an equivalent diameter as an average of the largest and smallest section diameters and an equivalent length equal to an average of the largest and smallest tuber lengths;
- Multidimensional heat transfer in the tubers idealised as a short cylinder can be using the product solution approach (Çengel and Ghajar, 2015; Christensen and Adler-Nissen, 2015).
- Heat transfer in the domain occurs by internal conduction and surface convection only;

**Table 2.** computed thermophysical properties of cocoyam tubers (Choi and Okos, 1986).

| Property | Units | Temperature, T (°C) | |
|---|---|---|---|
| | | 10 | 30 |
| Density (ρ) | $kg \cdot m^{-3}$ | 1125.96 | 1122.23 |
| Specific heat capacity ($C_p$) | $kJ \cdot kg^{-1} \cdot K^{-1}$ | 3.347 | 3.359 |
| Effective thermal conductivity ($k_{eff}$) | $W \cdot m^{-1} \cdot K^{-1}$ | 0.414 | 0.414 |
| Thermal diffusivity (α) | $m^2 \cdot s^{-1}$ | $1.099 \times 10^{-7}$ | $1.098 \times 10^{-7}$ |

- The introduction of effective heat transfer coefficients in the Biot number formulae enables the solution of the transient heat transfer problem using a modified lumped system approach (Xu et al., 2012).
- For the air velocity range studied, the external surface of each tuber is fully surrounded by the cooling air (Zou et al., 2006a).

#### 2.3.2. Governing equations for transient heat transfer analysis

Transient heat conduction with a convective boundary was studied using the one-term solution of the Fourier series which is a reasonable approximation of transient heat transfer (Çengel and Ghajar, 2015). During the harvesting of a cocoyam tuber, two wounds are inflicted on the tuber, one to trim the dry bottommost end and one at the petiole base to remove the foliage. The geometry of the trimmed tubers therefore closely resembles a cylinder. Cylindrical geometries where L/D < 1.85 are known as short cylinders (Bharti et al., 2007; Zdravkovich et al., 1989). The tubers utilised in this study had an L/D of 1.62 ± 0.31 and therefore fit the description of short cylinders. The solution for the temperature at any point in the body of a short cylinder with transient cooling is computed by superposing the solutions of an infinitely long cylinder with a finite radius ($r_o$) and an infinitely large slab with a finite thickness (2L) as shown in Figure 2.

For the infinite cylinder and infinite slab geometries, the temperature history is calculated from Eq. (1) (Çengel, 2015).

$$\Omega_i = \sum_{i=1}^{\infty} A_i \cdot e^{-\lambda_i^2 \cdot Fo} \tag{1}$$

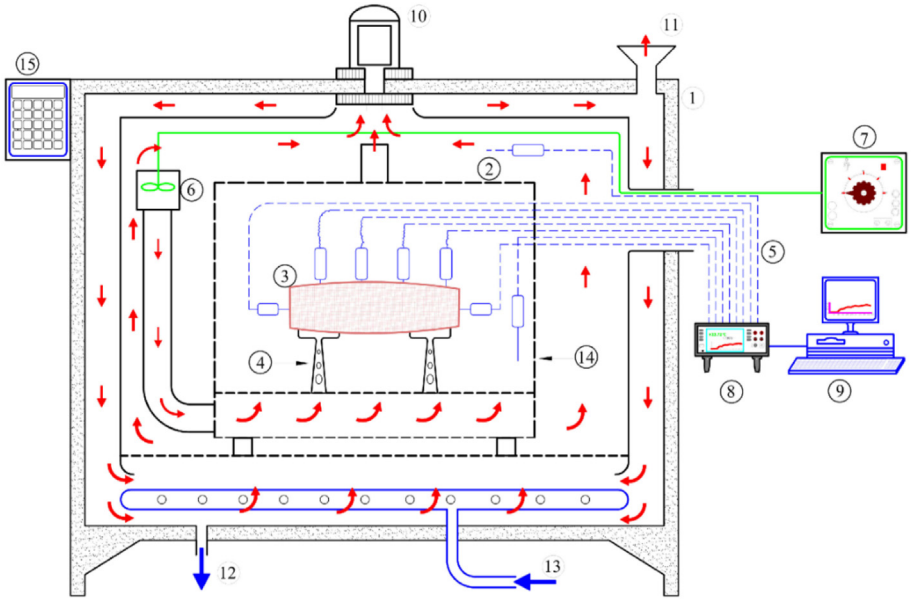


**Figure 1.** Experimental set-up (1. Vötsch VCL 400 Climate chamber, 2. RTD sensors, 3. Tuber, 4. Tuber support, 5. RTD wiring, 6. Ebmpapst Axial Suction Fan, 7. PHYWE Automatic Voltage/Speed regulator, 8. Keysight Data logger, 9. Logging computer, 10. Motor and Radial Blower Fan, 11. Vapour exhaust vent, 12. Condensate exhaust vent, 13. Distilled water inlet and humidifier, 14. Insulated test box, 15. Climate chamber control panel).

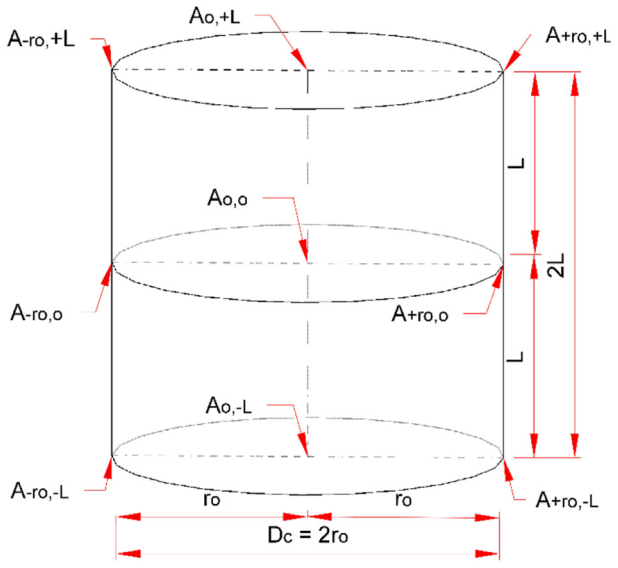


**Figure 2.** Dimension definitions of a short cylinder.

where: $\Omega_i$ = dimensionless temperature difference, $A_i$ = lag factor, $\lambda_i$ = eigen value, $\lambda_i^2$ = Fourier exponent, Fo = Fourier number, subscript i = number of terms in the solution.

The one-term approximated lag factors for cylinder ($A_{1.c}$) and slab geometries ($A_{1.s}$) are determined from Eqs. (2) and (3) (Çengel, 2015). The value of $r_o$ in Eq. (2) is equal to the radius of the tubers while r is the radius at any point of the tuber cross-section. In this study, the determination of the temperature history just under the skin of the tubers utilised $r = (r_o - t_s)$, where $t_s = 2$ mm is the thickness of the tuber skin. The value of L in Eq. (3) is equal to half the height/length of the tuber (i.e., L) as shown in Figure 2. The value of x is then the height at any point above or below the half-height of the tubers. Determination of the temperature history just at the surface of the trimmed ends of the tuber would be the case where x = L.

$$A_{1.c} = \frac{2 \cdot J_1(\lambda_{1.c})}{\lambda_{1.c} \cdot \left[J_0^2(\lambda_{1.c}) + J_1^2(\lambda_{1.c})\right]} \cdot J_0\left(\lambda_{1.c} \cdot \frac{r}{r_o}\right) \tag{2}$$

where: $A_{1.c}$ = lag factor for cylinder geometry, $\lambda_{1.c}$ = eigenvalue for cylinder geometry, subscript 1.c = one-term approximate for cylinder geometry, $J_0$ () and $J_1$ () are the Bessel functions of the first kind of order 0 and 1 respectively.

$$A_{1.s} = \frac{2 \cdot sin(\lambda_{1.s})}{\lambda_{1.s} + sin(\lambda_{1.s}) \cdot cos(\lambda_{1.s})} \cdot cos\left(\lambda_{1.s} \cdot \frac{x}{L}\right) \tag{3}$$

where: $A_{1.s}$ = lag factor for slab geometry, $\lambda_{1.s}$ = eigenvalue for slab geometry, subscript 1.s = one-term approximate for slab geometry.

Eqs. (2) and (3) are then substituted into Eq. (1) to obtain the one-term approximated dimensionless temperature differences for an infinite cylinder ($\Omega_{1.c}$) and infinite slab ($\Omega_{1.s}$) as given in Eqs. (4) and (5).

$$\Omega_{1.c} = \frac{2 \cdot J_1(\lambda_{1.c})}{\lambda_{1.c} \cdot \left[J_0^2(\lambda_{1.c}) + J_1^2(\lambda_{1.c})\right]} \cdot J_0\left(\lambda_{1.c} \cdot \frac{r}{r_o}\right) \cdot e^{-\lambda_{1.c}^2 \cdot Fo} \tag{4}$$

$$\Omega_{1.s} = \frac{2 \cdot sin(\lambda_{1.s})}{\lambda_{1.s} + sin(\lambda_{1.s}) \cdot cos(\lambda_{1.s})} \cdot cos\left(\lambda_{1.s} \cdot \frac{x}{L}\right) \cdot e^{-\lambda_{1.s}^2 \cdot Fo} \tag{5}$$

The Fourier number in Eqs. (1), (4), and (5) is also known as the dimensionless time and is determined using Eq. (6).

$$Fo = \frac{\alpha_c \cdot t}{S^2} \tag{6}$$

where: $\alpha_c$ = thermal diffusivity of tubers ($m^2 \cdot s^{-1}$), t = total cooling time (s), S = characteristic length (m) which is half radius for the cylinder geometry and half-thickness for the slab geometry.

The values of the eigenvalue ($\lambda$) and the Fourier exponent ($\lambda^2$) in Eqs. (4) and (5) are determined using Eqs. (7) and (8) by applying an iterative procedure as discussed in section 2.3.3 (Çengel, 2015).

$$Bi_c - \lambda \cdot \frac{J_1(\lambda)}{J_0(\lambda)} = 0 \tag{7}$$

where: $Bi_c$ = Biot number for cylinder geometry.

$$Bi_s - \lambda \cdot tan(\lambda) = 0 \tag{8}$$

where: $Bi_s$ = Biot number for slab geometry.

The values of $Bi_c$ and $Bi_s$ in Eqs. (7) and (8) are determined as functions of the effective convective heat transfer coefficient, the characteristic length and the effective thermal conductivity of the cocoyam tubers using Eqs. (9) and (10) following Xu et al. (2012).

$$Bi_c = \frac{h_{eff.c} \cdot (r_o/2)}{k_{eff}} \tag{9}$$

$$Bi_s = \frac{h_{eff.s} \cdot L}{k_{eff}} \tag{10}$$

where: $h_{eff.c}$ = effective heat transfer coefficient for cylindrical geometry, $h_{eff.s}$ = effective heat transfer coefficient for slab geometry, keff = effective thermal conductivity of the cocoyam tubers, $r_o$ = radius of cylinder geometry, L = half-thickness of slab geometry.

The effective heat transfer coefficients in Eqs. (9) and (10) are determined using Eqs. (11) and (12) respectively (Xu et al., 2012).

$$h_{eff.s} = \frac{1}{\frac{1}{h} + \frac{L}{3 \cdot k_{eff}}} \tag{11}$$

$$h_{eff.c} = \frac{1}{\frac{1}{h} + \frac{r_o}{4 \cdot k_{eff}}} \tag{12}$$

where: h = convective heat transfer coefficient.

The convective heat transfer coefficient in Eqs. (11) and (12) is determined as a function of Reynold's number (Re), Prandtl number (Pr) and the thermophysical properties of air obtained from Rohsenow et al. (1998). The convective heat transfer coefficient in Eqs. (11) and (12) is the overall heat transfer coefficient calculated using Eq. (13) (Çengel, 2015).

$$h = 0.683 \cdot \left(Re^{0.466} \cdot Pr^{1/3}\right) \cdot \frac{k_a}{D} \tag{13}$$

where: h = convective heat transfer coefficient, Re = Reynolds number, Pr = Prandtl number, $k_a$ = thermal conductivity of air, D = diameter of tuber (m).

The Reynolds number and Prandtl number in Eq. (13) are determined using Eqs. (14) and (15) respectively.

$$Re = \frac{\rho_a \cdot \vartheta_a \cdot D}{\mu_a} \tag{14}$$

$$Pr = \frac{C_{pa} \cdot \mu_a}{k_a} \tag{15}$$

where $\rho_a$ = density of air ($kg \cdot m^{-3}$), $\vartheta$ = cooling air velocity ($m \cdot s^{-1}$), $C_{pa}$ = Specific heat capacity ($kJ \cdot kg^{-1} \cdot K^{-1}$), $\mu_a$ = dynamic viscosity of air ($kg \cdot m^{-1} \cdot s^{-1}$).

The one-term approximated dimensionless temperature difference ($\Omega_{1.sc}$) for a short cylinder is obtained by calculating the product of the one-term approximated dimensionless temperature differences for an infinite cylinder ($\Omega_{1.c}$) in Eq. (4) and an infinite slab geometry ($\Omega_{1.s}$) in Eq. (5) as shown in Eq. (16).

$$\Omega_{1.sc} = \Omega_{1.c} \times \Omega_{1.s} \tag{16}$$

where: $\Omega_{1.sc}$ = one-term approximated temperature difference for short cylinder geometry. The one-term approximated dimensionless temperature difference for a short cylinder ($\Omega_{1.sc}$) can also be calculated using Eq. (17) (Çengel, 2015).

$$\Omega_{1.sc} = \frac{T_t - T_\infty}{T_i - T_\infty} \tag{17}$$

where $T_t$ = temperature at any point (r, x) in a short cylinder after a time, t, $T_i$ = initial temperature of raw tubers (°C), $T_\infty$ = temperature of cooling air (°C).

Rearranging Eq. (17), the temperature at any point of a short cylinder after a time, t, can be calculated using Eq. (18).

$$T_t = \Omega_{1.sc} \cdot (T_i - T_\infty) + T_\infty \tag{18}$$

The amount of field heat removed from each tuber at any time during the cooling process can be calculated using Eqs. (19), (20), (21), (22), and (23) (Çengel and Ghajar, 2015).

$$\left(\frac{Q}{Q_{max}}\right)_{sc} = \left(\frac{Q}{Q_T}\right)_c + \left(\frac{Q}{Q_T}\right)_s \cdot \left[1 - \left(\frac{Q}{Q_T}\right)_c\right] \tag{19}$$

where Q = field heat lost by the product to the surroundings after time, t (kJ), $Q_{max}$ = theoretical maximum heat content of the material (kJ), $(Q/Q_{max})_{sc}$ represents the ratio of the finite field heat removed in time, t, to the theoretical maximum heat content of the material for the short-cylinder geometry.

The second term on the right side of Eq. (20) represents the energy ratio for an infinite cylinder and is a function of the one-term approximated dimensionless temperature difference for an infinite cylinder ($\Omega_{1.c}$) and the eigenvalue ($\lambda_{1.c}$) (Çengel, 2015).

$$\left(\frac{Q}{Q_{max}}\right)_c = 1 - 2 \cdot \Omega_{1.c} \cdot \left(\frac{J_1(\lambda_{1.c})}{\lambda_{1.c}}\right) \tag{20}$$

where $(Q/Q_{max})_c$ represents the ratio of the finite field heat removed in time, t, to the theoretical maximum heat content of the material for the cylinder geometry.

The second term on the right side of Eq. (21) represents the energy ratio for an infinite slab geometry and is also a function of the one-term approximated dimensionless temperature difference for an infinite slab ($\Omega_{1.s}$) and the eigenvalue ($\lambda_{1.s}$) (Çengel, 2015).

$$\left(\frac{Q}{Q_{max}}\right)_s = 1 - \Omega_{1.s} \cdot \left(\frac{sin\ \lambda_{1.s}}{\lambda_{1.s}}\right) \tag{21}$$

where $(Q/Q_{max})_s$ represents the ratio of the finite field heat removed in time, t, to the theoretical maximum heat content of the material for the slab geometry.

The theoretical maximum heat content of the cocoyam tubers as used in Eqs. (19), (20), and (21) is calculated using Eq. (22).

$$Q_{max} = \rho \cdot V \cdot c_p \cdot (T_i - T_\infty) \tag{22}$$

where V = volume of tuber ($m^3$), ρ = density ($kg \cdot m^{-3}$), $c_p$ = specific heat capacity ($kJ \cdot kg^{-1} \cdot K^{-1}$).

The amount of field heat transferred across the domain after a time, t, is then calculated by substituting Eqs. (20), (21), and (22) into Eq. (19) to yield Eq. (23);

$$Q_{sc} = \rho \cdot V \cdot c_p \cdot (T_i - T_\infty) \cdot \left\{\left(\frac{Q}{Q_T}\right)_c + \left(\frac{Q}{Q_T}\right)_s \cdot \left[1 - \left(\frac{Q}{Q_T}\right)_c\right]\right\} \tag{23}$$

### 2.3.3. Simulation procedure

The simulation of the amount of time required for cocoyam tubers to cool to the target temperature was conducted in a series of sequential steps as shown in Figure 3. It should be observed that the calculation of the lag factors, eigenvalues and dimensionless temperature differences was a repetitive process that required iteration to obtain an accurate answer. A code was therefore written in the Python software (Python Software Foundation, Delaware, USA) to automate the process. From an initial guess of $\lambda_i = 0$ and $t = 0$, the script made increments of 0.0001 to $\lambda_i$ and 10 to $t$ until the difference between the Biot number and the second term of Eqs. (7) and (8) converged to 0 and the tuber temperature converged to 12 °C which is in the recommended storage temperature range of 11–13 °C (Opara, 1999).

### 2.3.4. Validation and method comparison

In the applied sciences, novel methods of measuring a phenomenon are often compared to standard methods to determine their validity and compatibility. In doing so, statistical tests are conducted to quantify deviations between the two methods and determine the influence of the deviations on subsequent predictions (Ungerer and Pretorius, 2017). While classical statistical metrics such as the correlation coefficient (r) and coefficient of determination ($r^2$) are popular, recent studies have criticized them as only being measures of linear association as opposed to actual agreement between data measured using two methods Giavarina (2015); Lin (1989). Novel techniques have been proposed to measure the agreement between datasets (Lin et al., 2002; Morley et al., 2018; Shrestha et al., 2020; Ungerer and Pretorius, 2017). In this study, the following robust metrics were used to determine the degree of agreement between the predictions and observations.

a) Symmetric Median Absolute Percentage Error (SMDAPE)

When comparing independent datasets from unrelated sources, utilisation of measures of accuracy that are independent of the scale of the data such as percentage errors is recommended (Morley et al., 2018). The Mean Absolute Percentage Error (MAPE) is a frequently utilised metric when the quantity to be predicted is known to be always positive (de Myttenaere et al., 2016). MAPE is popular because it is intuitively interpreted in terms of a relative error (de Myttenaere et al., 2016; Morley et al., 2018). However, Morley et al. (2018) propose the Symmetric Median Absolute Percentage Error (SMDAPE). SMDAPE is equally intuitive to interpret, penalizes over-prediction and under-prediction equally and is robust in the presence of outliers (Morley et al., 2018). The lower the value of SMDAPE, the closer the predictions to the observations (Morley et al., 2018; Swamidass, 2000). The FindErrors module in TSErrors 1.0 library of the Python software was used to compute the SMDAPE.

$$\text{SMDAPE} = 100 \cdot (\exp(\text{M}(|\log_e(\text{Q})|)) - 1) \tag{24}$$

where M = median, Q = ratio of prediction to observation

b) Huber regression

Huber regression is a commonly used method for robust regression to provide reliable regression results in the presence of outliers and high leverage points (Fox and Weisberg, 2012). This was achieved by minimizing the Mean Squared Error (MSE) in the Huber loss function (de Myttenaere et al., 2016; Huber, 1992). Assessment of agreement using regression coefficients involves testing the slope coefficient and the intercept coefficient against the ideal values of 1 and 0 respectively (Golbraikh and Tropsha, 2002). Values of the slope and intercept statistically different from 1 and 0 respectively indicate the presence of a systematic error (Altman and Bland, 1983).

In this study, the Huber regression was applied to determine the regression slope and intercept between the predictions and observations.

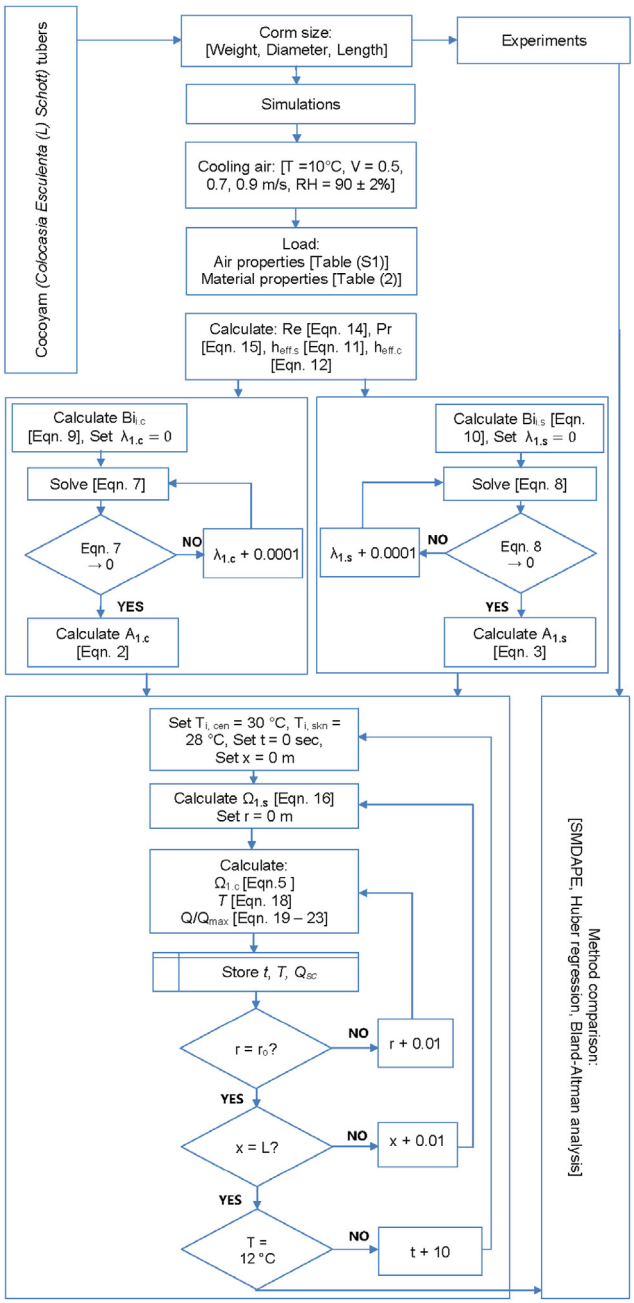


**Figure 3.** The simulation procedure.

The Huber Regressor class linear model in Python scikit-learn was applied to compute the robust slope and intercept of the regression model and to flag outliers (Pedregosa et al., 2011). The Huber loss function was fit with a value of epsilon of 1.0, which attempts to leave the fewest data points out of the fit for maximum robustness to outliers.

c) Bland-Altman analysis

Bland-Altman analysis quantifies the degree of agreement between two datasets under comparison using their deviations (Bland and Altman, 1999). The method evaluates the bias between the mean differences between predictions and observations and constructs limits of agreement within which 95 per cent of the differences should lie if a good agreement is present (Giavarina, 2015). For two datasets to be deemed to agree, the scattered deviations plotted on a Bland-Altman plot should lie between the upper and lower limits of agreement. The deviations should also be uniformly distributed on both sides of the mean difference and zero bias lines and heteroscedasticity should be absent (Bland and Altman, 1999).

The Bland-Altman method only establishes the limits of agreement but does not define whether those limits are acceptable or not (Giavarina, 2015). Therefore, acceptable limits of agreement should be defined from experience or established industry standards (Giavarina, 2015). In this study, Bland-Atman plots were constructed in Python software using the pyCompare module (Jake and Tirrell, 2020). The plots were then visually inspected for patterns and the absence of bias. An ideal agreement between predictions and observations is achieved when the Bland-Altman plots display accuracy (i.e., when the bias is zero or close to zero) and precision (i.e., when the LOA are close to the bias line) (Bland and Altman, 1999).

#### 2.3.5. Statistical analysis

The validity of the method comparison tests discussed relies on the basic assumption that the data follows a Gaussian distribution and that the variance is uniform. Before validation and method comparison, the datasets were subjected to the D'Agostino-Pearson test and histograms were constructed to confirm normality (D'Agostino and Pearson, 1973). The two datasets were also tested to confirm uniformity of variance using Levene's test (Levene, 1960). The Student's *t*-test for paired samples was also applied to get an initial assessment of the existence of bias. All statistical analyses were performed using the SciPy library in Python software (Virtanen et al., 2020).

## 3. Results and discussions

### 3.1. Heat transfer coefficient and biot number

#### 3.1.1. Heat transfer coefficient

Information on product heat transfer coefficients is critical in the design of food refrigeration systems (Kumar et al., 2008). Accurate prediction of the total cooling time and the corresponding cooling loads is contingent on the accurate estimation of the surface heat transfer coefficient (Becker and Fricke, 2004). Table 3 provides the convective heat transfer coefficients as calculated using Eqs. (11), (12), and (13). In this study, the surface heat transfer coefficients are calculated from Reynolds number and Prandtl number correlations. These correlations utilise the thermophysical properties of the cooling air and the dimensions of the tubers as inputs. With the density, viscosity, specific heat capacity and thermal conductivity as constant inputs, the surface heat transfer coefficient is therefore influenced by the air velocity, the radius, and the length of the tubers. This was confirmed by statistical analysis which found only the air velocity ($p < 0.0001$) and tuber size ($p < 0.0001$) to be influential at the 0.05 level of significance as opposed to the tuber orientation ($p > 0.05$). Small tubers exhibited higher values of the surface heat transfer coefficients than larger tubers.

#### 3.1.2. Biot number

The Biot number is a dimensionless quantity that provides information on the controlling mechanism of heat transfer (Becker and Fricke, 2004; Giner et al., 2010; van der Sman, 2003). When the internal resistance is less than 10 per cent of the external resistance to heat transfer (i.e., $Bi < 0.1$), lumped system analysis could be applied for transient heat transfer analysis (Çengel and Ghajar, 2015; Chen, 2005). In this study, the Biot number was significantly influenced by the air velocity ($p < 0.0001$) and the tuber size ($p < 0.0001$) but not the orientation to airflow ($p > 0.05$). Çengel and Ghajar (2015) report that small-sized bodies in a medium such as air which is a poor conductor of heat exhibit relatively lower values of the Biot number. A similar finding was obtained for sweet potatoes where lower values of the Biot number corresponded with medium-sized sweet potato roots and slower air velocities (Korese et al., 2017).

Table 4 provides the calculated values of Bi with the tubers idealised as infinite cylinders and infinite slabs. In this study, the values of Bi range from 0.26 – 0.43 for cylindrical geometries and 0.83–1.69 for slab geometries respectively. These values are on average 3–13 times greater

**Table 3.** Heat transfer coefficients (Mean ± SD).

| Orientation | $\vartheta_a$ (m·s$^{-1}$) | Tuber size | h (W·m$^{-2}$·K$^{-1}$) | | |
|---|---|---|---|---|---|
| | | | $h_{overall}$ | $h_{eff,c}$ | $h_{eff,s}$ |
| across | 0.5 | small | 8.63 ± 1.10 | 7.63 ± 0.85 | 6.73 ± 0.63 |
| | | large | 7.96 ± 0.52 | 6.68 ± 0.41 | 5.87 ± 0.74 |
| | 0.7 | small | 10.78 ± 0.43 | 9.20 ± 0.31 | 7.49 ± 0.07 |
| | | large | 9.13 ± 0.42 | 7.62 ± 0.30 | 6.85 ± 0.25 |
| | 0.9 | small | 11.84 ± 1.11 | 10.00 ± 0.95 | 8.75 ± 0.23 |
| | | large | 10.26 ± 0.74 | 8.50 ± 0.58 | 6.57 ± 0.57 |
| along | 0.5 | small | 9.61 ± 0.20 | 8.46 ± 0.09 | 7.40 ± 0.01 |
| | | large | 7.65 ± 0.18 | 6.47 ± 0.17 | 5.82 ± 0.12 |
| | 0.7 | small | 11.40 ± 0.91 | 9.69 ± 0.87 | 8.39 ± 0.38 |
| | | large | 9.70 ± 0.15 | 8.06 ± 0.14 | 6.53 ± 0.00 |
| | 0.9 | small | 12.40 ± 0.16 | 10.42 ± 0.16 | 8.76 ± 0.34 |
| | | large | 10.82 ± 0.26 | 8.92 ± 0.25 | 7.11 ± 0.45 |

than 0.1. This signifies that temperature distribution in the tubers is non-uniform and therefore the internal resistance to heat conduction is substantial. Therefore, classical lumped system analysis of transient heat transfer is invalid. However, when the effective convective heat transfer coefficients were introduced in the Biot number formulae, effective Biot numbers were calculated and the heat transfer problem was solved directly using a modified lumped system approach (Xu et al., 2012).

### 3.2. Cooling kinetics and cooling time

#### 3.2.1. Cooling kinetics

The efficiency of cooling operations for food products is dependent on the proper design of cooling equipment to suit the requirements of the particular cooling application (Becker and Fricke, 2004). Cooling kinetics provide important design information for the prediction of the amount of time required to cool a product to its target temperature (Carroll et al., 1996). In turn, the cooling time helps in the estimation of the corresponding cooling loads (Becker and Fricke, 2004). Cooling kinetics are therefore an important design and management tool for cooling applications. Figure (4a) and Figure (4b) illustrate the change in temperature with time at the core and under the skin of tubers respectively. The curves portray an exponential decay behaviour with a rapid cooling rate at the start of the cooling process which levels off towards the end of cooling. Similar behaviour was observed during the cooling of sweet potatoes (Korese et al., 2017), grapes (Dincer, 1995), southern bluefin tuna (Davey, 2015), oranges and tomatoes (Kumar et al., 2008). Notably, the curves for predictions closely mimic the observations further confirming the comparability of the datasets.

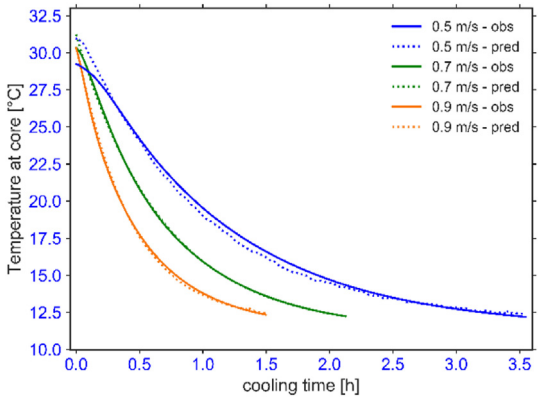


**Figure (4a).** Cooling kinetics at the core (small size, across orientation).

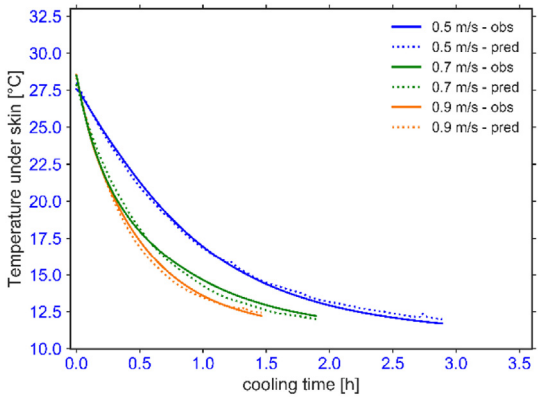


**Figure 4b.** Cooling kinetics under the skin (small size, across orientation).

#### 3.2.2. Cooling time

For cooling applications, the velocity of the cooling air flowing past the product is the most significant factor influencing the surface heat transfer coefficient which in turn influences the length of the cooling process (Becker and Fricke, 2004). As shown in Figure (5a) and Figure (5b), the air velocity significantly influenced the amount of time required to attain 12 °C both at the core ($p < 0.05$) and just under the skin ($p < 0.05$) of the tubers. Increasing the air velocity significantly reduced the total amount of time required to cool the tubers to the final temperature of 12 °C. This agrees well with the findings of Dehghannya et al. (2010), Dincer (1995), Gaffney and Baird (1977) and Kumar et al. (2008).

**Table 4.** Biot numbers (Mean ± SD).

| Orientation | $\vartheta_a$ (m·s$^{-1}$) | Tuber size | infinite cylinder | | infinite slab | |
|---|---|---|---|---|---|---|
| | | | D (mm) | $Bi_{eff,c}$ | L (mm) | $Bi_{eff,s}$ |
| across | 0.5 | small | 49.25 ± 1.00 | 0.26 ± 0.04 | 79.75 ± 2.75 | 0.83 ± 0.13 |
| | | large | 79.63 ± 3.38 | 0.38 ± 0.01 | 116.25 ± 13.75 | 1.10 ± 0.25 |
| | 0.7 | small | 52.75 ± 0.25 | 0.34 ± 0.02 | 90.50 ± 0.50 | 1.32 ± 0.13 |
| | | large | 72.00 ± 0.50 | 0.40 ± 0.02 | 101.00 ± 6.00 | 1.00 ± 0.04 |
| | 0.9 | small | 52.13 ± 5.38 | 0.37 ± 0.00 | 72.50 ± 12.50 | 1.05 ± 0.28 |
| | | large | 66.88 ± 3.38 | 0.41 ± 0.01 | 137.25 ± 15.25 | 1.69 ± 0.07 |
| along | 0.5 | small | 51.50 ± 2.00 | 0.29 ± 0.26 | 85.00 ± 2.00 | 0.90 ± 0.09 |
| | | large | 79.00 ± 3.50 | 0.36 ± 0.01 | 102.25 ± 1.25 | 0.94 ± 0.01 |
| | 0.7 | small | 52.25 ± 7.75 | 0.36 ± 0.02 | 77.50 ± 4.00 | 1.07 ± 0.14 |
| | | large | 69.50 ± 2.00 | 0.41 ± 0.01 | 124.00 ± 4.00 | 1.45 ± 0.07 |
| | 0.9 | small | 50.75 ± 1.25 | 0.38 ± 0.00 | 83.50 ± 8.50 | 1.25 ± 0.11 |
| | | large | 65.50 ± 3.00 | 0.43 ± 0.01 | 121.25 ± 16.75 | 1.58 ± 0.18 |

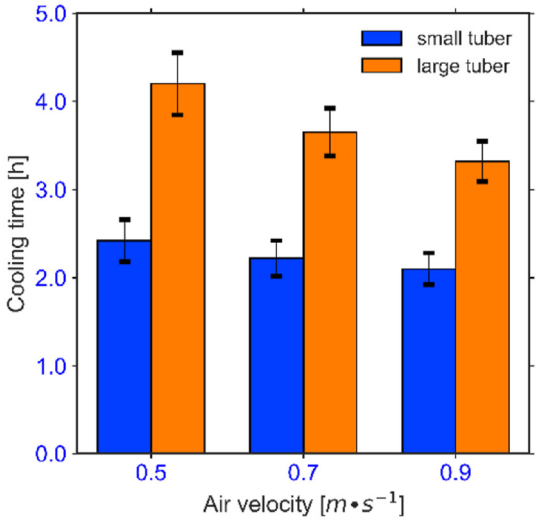


**Figure 5a.** Cooling time against air velocity at the core.

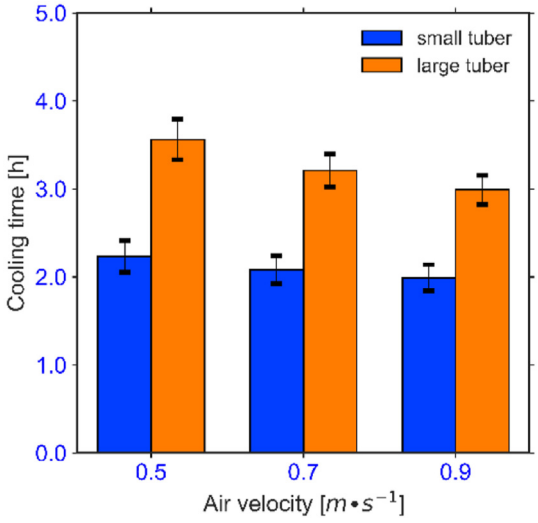


**Figure 5b.** Cooling time against air velocity under the skin.

Knowledge of the influence of product size is critical in deciding the best strategy for the reduction of cooling time. This is because product size has a significant influence on the heat transfer coefficients (Dehghannya et al., 2010; Dincer and Genceli, 1994; Wang et al., 2001). In the case where the internal resistance to heat transfer supersedes the external resistance, a better result can be achieved by reducing product dimensions as compared to reducing the size of packaging or increasing air velocity (Glavina, Di Scala, & del Valle, 2007; Pham, 2002). This is despite the fact that the smaller sized biological products exhibit higher respiration rates and therefore increased loss of moisture (Haagenson et al., 2006). As shown in Figure (5a) and Figure (5b), tuber size significantly influenced the amount of time required to attain 12 °C both at the core ($p < 0.0001$) and just under the skin ($p < 0.0001$) of the tubers. The influence of the tuber size on the cooling time was observed to be greater than that of the air velocity. Small-sized tubers required less time to cool to the target temperature as compared to the large-sized tubers. Similar behaviour has been reported for potatoes (Glavina et al., 2007) and sweet potatoes (Korese et al., 2017). The orientation of the tubers to the airflow can be intuitively understood to change the shape of the tubers depending on the tuber face perpendicular to the airflow. During forced air cooling of agricultural products, the shape of the product is known to influence the heat transfer coefficients (Becker and Fricke, 2004). However, this study found the tuber orientation to airflow (tuber shape) to neither influence the heat transfer coefficients nor the cooling time at the core and under the skin ($p > 0.05$). Table 5 compares the cooling time determined from the prediction model to experimental data. Additional statistical comparison results of the predictions and observations are provided as supplementary data. While varying differences can be observed for each pair of predictions and observations, the Student's *t*-test reveals that the overall means of the differences between two datasets are not statistically different at the 0.05 level of significance.

### 3.3. Field heat removed from tubers

Forced convection cooling is a critical undertaking commonly applied to agricultural produce after harvest to remove the field heat and to provide favourable conditions for storage (Defraeye et al., 2014). This is because the quality of the produce after harvest and the storage time is highly influenced by the product temperature and in extension the sensible heat content. The amount of heat removed from a product to its surroundings throughout cooling is equivalent to the change in the energy content of the product (Çengel and Ghajar, 2015). This quantity contributes to the cooling load but is different from the energy required to precool the air and to run the ventilation system (Ndisya et al., 2021). Information on the cooling load is pertinent in the design and operation of the cooling system (Dincer, 2003).

Figure 6 and Table 6 provide the amount of energy removed from the tubers by cooling as determined using the method proposed by Çengel and Ghajar (2015). The amount of the field heat removed was significantly influenced by the tuber size ($p < 0.0001$) but not the air velocity and the tuber orientation to airflow ($p > 0.05$). On average, large-sized tubers contained approximately 55.6 per cent more energy than small-sized tubers. Since the temperature difference and the thermophysical properties of the cocoyam material are assumed to be constant in the modelling process, the field heat content is therefore solely influenced by the weight of the tubers. As shown in Eq. (22), the weight of the tubers is represented as a product of the tuber density and volume and is directly proportional to the energy content. Therefore, an increase in the tuber size from small to large corresponds to an increase in the field heat to be removed.

### 3.4. Validation and method comparison

Tables 7 and 8 present the robust estimates of the Huber regression coefficients at the core and under the skin of the tubers. The regression coefficients depict minor deviations from the expected ideal values of a slope of 1 and an intercept of 0. However, t-test results on the mean values of the regression coefficients as presented in Table 9 reveal that the overall values of slope and intercept are not significantly different from 1 and 0 respectively at the 0.05 level of significance. These findings reveal the linear relationship between the predictions and observation and therefore the high degree of agreement between the two datasets. Moreover, the values of SMDAPE presented in Tables 7 and 8 are in the range of 0.85–3.73 per cent at the core of the tubers and 0.94–2.91 per cent under the skin of the tubers. Conversion of the SMDAPE values to actual temperature deviation shows that the differences between model predictions and observations are in the range 0.26–1.12 °C at the commencement of the cooling process (i.e., at 30 °C) and 0.10–0.45 °C at the end of cooling (i.e., at 12 °C) at the core of the tubers. The corresponding temperature deviations under the skin of the tubers are in the range 0.28–0.87 °C at the start of cooling (i.e., 30 °C) and 0.11–0.35 °C at the end of cooling (i.e., 12 °C). If a maximum temperature deviation of 2 °C is acceptable, the model can be used interchangeably or in the place of direct experimental measurements.

Figure 7 presents exemplary Bland-Altman plots at the core and under the skin of the tubers. For the purposes of this study, the theoretical limits of agreement are set to be equal to ±2 °C, which is a variation that can be

**Table 5.** Average time to attain $T = 12 \pm 0.2$ °C at the core and under the skin (Mean ± SD).

| Orientation | $\vartheta_a$ (m·s$^{-1}$) | Tuber size | At the core | | Under the skin | |
|---|---|---|---|---|---|---|
| | | | Pred (h) | Obs (h) | Pred (h) | Obs (h) |
| across | 0.5 | small | 2.57 ± 0.46 | 2.38 ± 0.36 | 2.29 ± 0.24 | 2.35 ± 0.19 |
| | | large | 4.37 ± 0.00 | 3.56 ± 0.81 | 3.18 ± 0.00 | 3.18 ± 0.83 |
| | 0.7 | small | 2.13 ± 0.00 | 2.00 ± 0.27 | 1.93 ± 0.09 | 1.92 ± 0.08 |
| | | large | 2.96 ± 0.03 | 2.80 ± 0.16 | 2.72 ± 0.15 | 2.63 ± 0.06 |
| | 0.9 | small | 2.13 ± 0.00 | 1.86 ± 0.17 | 2.09 ± 0.00 | 2.01 ± 0.42 |
| | | large | 3.18 ± 0.00 | 3.79 ± 0.68 | 3.03 ± 0.00 | 3.04 ± 0.13 |
| along | 0.5 | small | 2.35 ± 0.03 | 2.35 ± 0.09 | 2.22 ± 0.04 | 2.19 ± 0.10 |
| | | large | 3.98 ± 0.00 | 3.25 ± 0.14 | 3.22 ± 0.00 | 3.23 ± 0.14 |
| | 0.7 | small | 2.23 ± 0.00 | 2.41 ± 0.11 | 2.15 ± 0.00 | 2.17 ± 0.11 |
| | | large | 3.85 ± 0.39 | 3.40 ± 0.24 | 3.39 ± 0.02 | 3.30 ± 0.04 |
| | 0.9 | small | 2.00 ± 0.00 | 2.22 ± 0.20 | 1.97 ± 0.11 | 1.91 ± 0.17 |
| | | large | 3.69 ± 0.37 | 3.33 ± 0.22 | 3.26 ± 0.00 | 3.17 ± 0.14 |

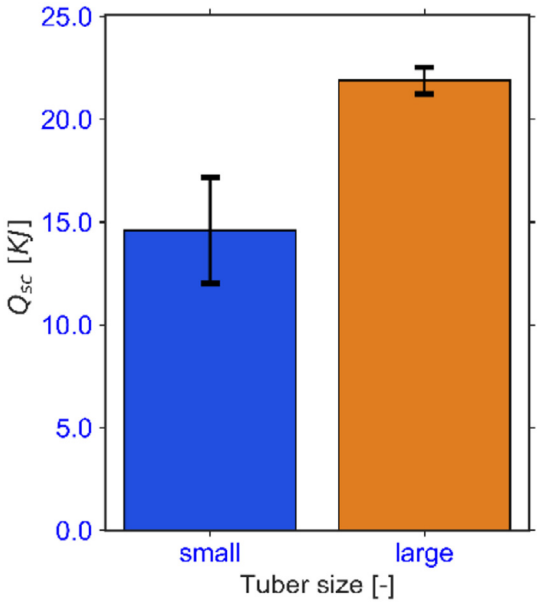


**Figure 6.** Field heat removed from tubers (0.7 m s$^{-1}$, small, across orientation).

reasonably tolerated in a bulk storage of well-cured cocoyam tubers (Opara, 1999). It can be observed that the limits of agreement for each case are narrower than the proposed theoretical limits of agreement. Further, the scattered differences lie inside the limits of agreement and their distribution on both sides of the mean difference line is approximately proportionate. However, Figure 7 as read together with Table (10) reveals the existence of minor systematic and proportional biases. In the Bland-Altman plots, the systematic bias is quantitatively equal to the mean difference while the proportional bias is depicted by the notably curvy scatter lines of differences. This is probably due to imprecise placement of the temperature sensors inside the tubers and spatial variation in the thermophysical properties of the cocoyam material. Differences in tolerances and errors in the instruments utilised to

**Table 6.** Field heat removed from tubers (Mean ± SD).

| Orientation | $\vartheta_a$ (m·s$^{-1}$) | small tubers | | large tubers | |
|---|---|---|---|---|---|
| | | Weight (g) | $Q_{sc}$ (kJ) | Weight (g) | $Q_{sc}$ (kJ) |
| across | 0.5 | 160.70 ± 5.92 | 10.17 ± 0.48 | 526.72 ± 42.05 | 24.78 ± 0.00 |
| | 0.7 | 219.77 ± 24.19 | 14.59 ± 2.59 | 381.00 ± 4.02 | 21.88 ± 0.65 |
| | 0.9 | 152.57 ± 7.76 | 9.61 ± 0.36 | 510.30 ± 13.17 | 31.90 ± 4.75 |
| along | 0.5 | 175.39 ± 10.14 | 12.08 ± 0.00 | 478.58 ± 36.10 | 27.45 ±1.25 |
| | 0.7 | 164.00 ± 26.09 | 12.40 ± 3.11 | 479.46 ± 15.64 | 30.11 ± 0.00 |
| | 0.9 | 168.09 ± 27.11 | 13.36 ± 0.00 | 425.84 ± 8.79 | 28.02 ± 4.64 |

**Table 7.** Model performance metrics at the core (Mean ± SD).

| Orient | $\vartheta_a$ (m·s$^{-1}$) | Tuber size | Huber regression $\hat{y}_{pred} = \beta_0 + \beta_1 \cdot \hat{y}_{obs}$ | | SMDAPE (%) |
|---|---|---|---|---|---|
| | | | $\beta_0$ | $\beta_1$ | |
| across | 0.5 | small | 0.62 ± 0.58 | 1.69 ± 0.05 | 1.60 ± 0.33 |
| | | large | −0.50 ±1.52 | 1.99 ± 0.55 | 1.96 ± 0.69 |
| | 0.7 | small | −0.63 ± 1.50 | 2.29 ± 0.87 | 2.45 ± 1.01 |
| | | large | 0.37 ± 0.05 | 1.50 ± 0.13 | 1.64 ± 0.23 |
| | 0.9 | small | −0.31 ± 0.00 | 0.82 ± 0.00 | 0.85 ± 0.00 |
| | | large | 0.16 ± 0.34 | 3.49 ± 0.25 | 3.74 ± 0.21 |
| along | 0.5 | small | 0.09 ± 0.15 | 1.70 ± 0.06 | 1.99 ± 0.11 |
| | | large | 0.51 ± 0.00 | 1.24 ± 0.00 | 1.21 ± 0.00 |
| | 0.7 | small | −0.04 ± 0.49 | 2.00 ± 0.30 | 1.99 ± 0.30 |
| | | large | 1.00 ± 0.84 | 2.63 ± 1.75 | 2.50 ± 1.77 |
| | 0.9 | small | −1.00 ± 0.88 | 2.40 ± 0.52 | 2.38 ± 0.63 |
| | | large | −0.80 ± 1.93 | 2.31 ± 0.68 | 2.26 ± 0.75 |

**Table 8.** Model performance metrics under the skin (Mean ± SD).

| Orient | $\vartheta_a$ (m·s$^{-1}$) | Tuber size | Huber Regression $\hat{y}_{pred} = \beta_0 + \beta_1 \cdot \hat{y}_{obs}$ | | SMDAPE (%) |
|---|---|---|---|---|---|
| | | | $\beta_0$ | $\beta_1$ | |
| across | 0.5 | small | −0.21 ± 1.14 | 1.01 ± 0.07 | 1.45 ± 0.04 |
| | | large | −0.82 ± 0.13 | 1.05 ± 0.00 | 1.12 ± 0.36 |
| | 0.7 | small | −1.03 ± 0.25 | 1.08 ± 0.01 | 1.86 ± 0.20 |
| | | large | −0.50 ± 0.21 | 1.03 ± 0.01 | 0.94 ± 0.32 |
| | 0.9 | small | −0.13 ± 0.00 | 1.00 ± 0.00 | 1.35 ± 0.00 |
| | | large | −0.46 ± 0.32 | 1.02 ± 0.02 | 1.47 ± 0.51 |
| Along | 0.5 | small | -0.71 ± 0.04 | 1.05 ± 0.01 | 1.35 ± 0.09 |
| | | large | −1.02 ± 0.00 | 1.07 ± 0.00 | 1.16 ± 0.00 |
| | 0.7 | small | −0.87 ± 0.94 | 1.05 ± 0.06 | 2.19 ± 0.48 |
| | | large | −1.43 ± 0.89 | 1.09 ± 0.06 | 1.66 ± 0.45 |
| | 0.9 | small | −1.48 ± 0.01 | 1.09 ± 0.01 | 2.91 ± 0.69 |
| | | large | −0.47 ± 0.09 | 1.03 ± 0.00 | 1.08 ± 0.03 |

**Table 9.** Student's t-test results.

| Sensor location | Huber Regression | | | | Bland-Altman | |
|---|---|---|---|---|---|---|
| | $\overline{\beta_0}$ | $\overline{\beta_0}$- 95% C.I [LCL, UCL] | $\overline{\beta_1}$ | $\overline{\beta_1}$ - 95% C.I [LCL, UCL] | *Mean diff.* | 95% C.I [LCL, UCL] |
| At the core | −0.06 | [−2.31, 2.19][b] | 0.99 | [0.82, 1.15][b] | 0.09 | [−0.46, 0.63][b] |
| Under the skin | −0.78 | [−2.10, 0.55][b] | 1.05 | [0.96, 1.14][b] | 0.15 | [−0.42, 0.72][b] |

Statistical significance: $H_0$: $\beta_0$.LCL <0 < $\beta_0$.UCL and $\beta_1$.LCL <1 < $\beta_1$.UCL, [a]p < 0.05 = significant, [b]p = non-significant.

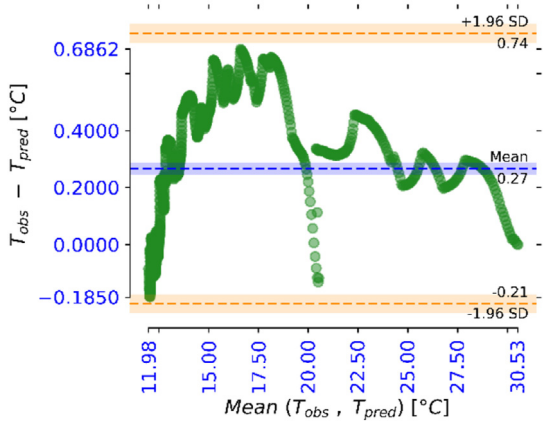


**Figure 7a.** Bland-Altman plots at the core (small size, across orientation, ϑ = 0.9 m $s^{-1}$).

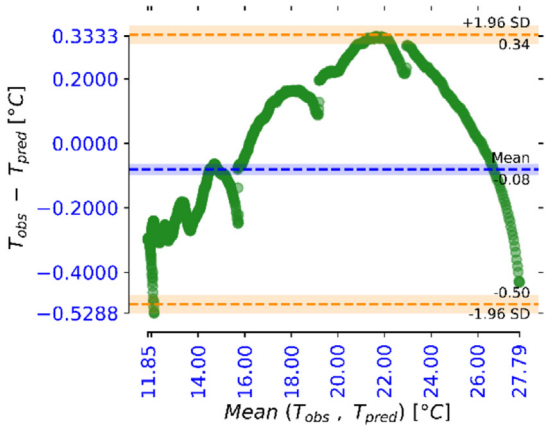


**Figure 7b.** Bland-Altman plots under the skin (small size, across orientation, ϑ = 0.9 m $s^{-1}$).

take measurements could also have contributed to biases. Nonetheless, this is a common challenge that has been acknowledged and discussed in other studies (da Silva et al., 2010; Korese et al., 2017). However, Table 9 and Table 10 show that the biases observed in this study are less than the tolerable maximum variation of ±2 °C and the overall mean bias is statistically not different from zero within the 0.05 level of significance. This variation could therefore be disregarded in practice.

## 4. Conclusions

The development of suitable cooling solutions requires the knowledge of how the thermophysical properties of a product interact with the temperature, velocity, and relative humidity of the cooling medium. To achieve wider utilisation in a practical setting such as on-farm precooling and storage, simple and computationally convenient mathematical models can be utilised to eliminate the need for expensive experiments and proprietary software. This study modelled the transient heat transfer process during forced convection cooling of whole cocoyam tubers using theories and standard formulae that are well established in literature.

Comparison of the prediction results to experimental data shows that the model can be utilised to reliably predict the cooling time and field heat content that can be expected when whole cocoyam tubers are subjected to forced convection cooling. Moreover, this study reveals that air velocity and tuber size are significant factors that should be adequately controlled to optimize the cooling process. The total cooling time decreased in the range 154.2–127.8 min for small tubers and 262.2–190.8 min for large tubers between the lower setting and the upper setting of the air velocity while the field heat removed ranged from 9.61 – 10.17 kJ for small tubers and 24.78–31.90 kJ for large tubers in the range of air velocity investigated. These findings demonstrate that increasing air velocity and utilising small-sized tubers could result in decreased cooling time and reduced field heat load. While it could be possible to control the size of the tubers to a certain degree through selective breeding, it is impossible to predict the exact sizes of tubers to expect from a farm. An immediate solution would be to sort the tubers by size to guarantee the validity of the model. This study has provided a basis for the determination of heat transfer in individual cocoyam tubers,

**Table 10.** Bland-Altman mean differences and limits of agreement (Mean ± SD).

| Orient. | $\vartheta_a$ (m·$s^{-1}$) | Tuber size | At the core | | | Under the skin | | |
|---|---|---|---|---|---|---|---|---|
| | | | *Mean diff. (°C)* | *U.LOA (°C)* | *L.LOA (°C)* | *Mean diff. (°C)* | *U.LOA (°C)* | *L.LOA (°C)* |
| across | 0.5 | small | −0.07 ± 0.01 | 0.51 ± 0.17 | −0.65 ± 0.15 | −0.31 ± 0.04 | 0.07 ± 0.05 | −0.69 ± 0.14 |
| | | large | −0.01 ± 0.07 | 0.54 ± 0.15 | −0.54 ± 0.02 | 0.12 ± 0.04 | 0.68 ± 0.26 | −0.46 ± 0.33 |
| | 0.7 | small | 0.58 ± 0.46 | 1.29 ± 0.53 | −0.53 ± 0.39 | 0.12 ± 0.02 | 1.07 ± 0.41 | −0.83 ± 0.38 |
| | | large | 0.03 ± 0.06 | 0.44 ± 0.09 | −0.39 ± 0.02 | 0.13 ± 0.09 | 0.81 ± 0.10 | −0.56 ± 0.07 |
| | 0.9 | small | 0.14 ± 0.00 | 0.57 ± 0.00 | −0.29 ± 0.00 | 0.22 ± 0.00 | 0.34 ± 0.00 | −0.29 ± 0.00 |
| | | large | 0.10 ± 0.03 | 0.62 ± 0.25 | −0.43 ± 0.31 | 0.45 ± 0.01 | 1.71 ± 0.12 | −0.82 ± 0.11 |
| along | 0.5 | small | −0.09 ± 0.12 | 0.64 ± 0.12 | −0.82 ± 0.12 | 0.31 ± 0.00 | 0.68 ± 0.11 | −0.16 ± 0.11 |
| | | large | −0.11 ± 0.00 | 0.43 ± 0.00 | −0.66 ± 0.00 | 0.09 ± 0.00 | 0.74 ± 0.00 | −0.55 ± 0.00 |
| | 0.7 | small | 0.41 ± 0.31 | 1.42 ± 0.22 | −0.61 ± 0.40 | 0.20 ± 0.16 | 0.83 ± 0.03 | −0.43 ± 0.35 |
| | | large | −0.11 ± 0.15 | 0.81 ± 0.26 | −1.03 ± 0.55 | 0.80 ± 0.69 | 1.36 ± 0.96 | −1.14 ± 0.41 |
| | 0.9 | small | 0.09 ± 0.19 | 1.35 ± 0.21 | −1.18 ± 0.17 | 0.17 ± 0.11 | 1.14 ± 0.40 | −0.82 ± 0.61 |
| | | large | 0.04 ± 0.04 | 0.50 ± 0.04 | −0.49 ± 0.11 | 0.32 ± 0.21 | 1.22 ± 0.30 | −0.59 ± 0.11 |

however, further generalisation for application to bulk tuber storage will inform the next phase of investigations.

## Declarations

### Author contribution statement

John Ndisya: Conceived and designed the experiments; Performed the experiments; Analyzed and interpreted the data; Wrote the paper.

Ayub Gitau; Duncan Mbuge; Barbara Sturm; Oliver Hensel: Analyzed and interpreted the data; Contributed reagents, materials, analysis tools or data; Wrote the paper.

Franz Roman: Conceived and designed the experiments; Performed the experiments; Analyzed and interpreted the data.

### Funding statement

Dr John Ndisya was supported by Deutscher Akademischer Austauschdienst [91692333].

This work was funded by the UPGRADE Plus project [323-06.01-03-2816PROC01] supported by the German Federal Ministry of Food and Agriculture (BMEL) and executed through the Federal Office for Agriculture and Food Germany (BLE).

### Data availability statement

Data will be made available on request.

### Declaration of interest's statement

The authors declare no competing interests.

### Additional information

No additional information is available for this paper.

## References

Aboubakar, Njintang, N.Y., Scher, J., Mbofung, C.M.F., 2009. Texture, microstructure and physicochemical characteristics of taro (Colocasia esculenta) as influenced by cooking conditions. J. Food Eng. 91 (3), 373–379.

Afolabi, T.J., Tunde-Akintunde, T.Y., Adeyanju, J.A., 2015. Mathematical modeling of drying kinetics of untreated and pretreated cocoyam slices. J. Food Sci. Technol. 52 (5), 2731–2740.

Altman, D.G., Bland, J.M., 1983. Measurement in medicine: the analysis of method comparison studies. The Statistician 32 (3), 307.

Barnhart, H.X., Lokhnygina, Y., Kosinski, A.S., Haber, M., 2007. Comparison of concordance correlation coefficient and coefficient of individual agreement in assessing agreement. J. Biopharm. Stat. 17 (4), 721–738.

Basediya, A., Samuel, D.V.K., Beera, V., 2013. Evaporative cooling system for storage of fruits and vegetables - a review. J. Food Sci. Technol. 50 (3), 429–442.

Becker, B.R., Fricke, B.A., 2004. Heat transfer coefficients for forced-air cooling and freezing of selected foods. Int. J. Refrig. 27 (5), 540–551.

Bharti, R.P., Chhabra, R.P., Eswaran, V., 2007. Steady forced convection heat transfer from a heated circular cylinder to power-law fluids. Int. J. Heat Mass Tran. 50 (5–6), 977–990.

Bland, J.M., Altman, D.G., 1999. Measuring agreement in method comparison studies. Stat. Methods Med. Res. 8 (2), 135–160.

Carroll, N., Mohtar, R., Segerlind, L.J., 1996. Predicting the cooling time for irregular shaped food products. J. Food Process. Eng. 19 (4), 385–401.

Çengel, Y., Ghajar, A., 2015. Heat and Mass Transfer: Fundamentals and Applications, fifth ed. McGraw-Hill Education, New York, USA.

Chen, X.D., 2005. Air drying of food and biological materials—modified Biot and lewis number analysis. Dry. Technol. 23 (9–11), 2239–2248.

Choi, Y., Okos, M., 1986. Effects of temperature and composition on the thermal properties of foods. Food Engineering and Process Applications 1, 93–101.

Christensen, M.G., Adler-Nissen, J., 2015. Simplified equations for transient heat transfer problems at low Fourier numbers. Appl. Therm. Eng. 76, 382–390.

D'Agostino, R., Pearson, E.S., 1973. Tests for departure from normality. Empirical results for the distributions of b2 and $\sqrt{}$ b1. Biometrika 60 (3), 613–622. Retrieved from. http://www.jstor.org/stable/2335012.

da Silva, W.P., e Silva, C.M.D.P.S., de O. Farias, V.S., e Silva, D.D.P.S., 2010. Calculation of the convective heat transfer coefficient and cooling kinetics of an individual fig fruit. Heat Mass Tran. 46 (3), 371–380.

Davey, K.R., 2015. Development and illustration of a computationally convenient App for simulation of transient cooling of fish in ice slurry at sea. LWT - Food Sci. Technol. (Lebensmittel-Wissenschaft -Technol.) 60 (1), 308–314.

de Myttenaere, A., Golden, B., Le Grand, B., Rossi, F., 2016. Mean Absolute percentage error for regression models. Neurocomputing 192, 38–48.

Defraeye, T., Lambrecht, R., Delele, M.A., Tsige, A.A., Opara, U.L., Cronjé, P., et al., 2014. Forced-convective cooling of citrus fruit: cooling conditions and energy consumption in relation to package design. J. Food Eng. 121, 118–127.

Dehghannya, J., Ngadi, M., Vigneault, C., 2010. Mathematical modeling procedures for airflow, heat and mass transfer during forced convection cooling of produce: a review. Food Eng. Rev. 2 (4), 227–243.

Dincer, I., 1994. Heat transfer coefficients for slab shaped products subjected to heating. Int. Commun. Heat Mass Tran. 21 (2), 307–314.

Dincer, I., 1995. Air flow precooling of individual grapes. J. Food Eng. 26 (2), 243–249.

Dincer, I., 1997. In: Haefner, L., Prescott, M. (Eds.), Heat Transfer in Food Cooling Applications, first ed. CRC Press.

Dincer, I., 2003. Refrigeration Systems and Applications. Wiley, West Sussex, England.

Dincer, I., Genceli, O.F., 1994. Cooling process and heat transfer parameters of cylindrical products cooled both in water and in air. Int. J. Heat Mass Tran. 37 (4), 625–633.

Elansari, A.M., Mostafa, Y.S., 2020. Vertical forced air pre-cooling of orange fruits on bin: effect of fruit size, air direction, and air velocity. Journal of the Saudi Society of Agricultural Sciences 19 (1), 92–98.

Fern, K., 2018. Useful Tropical Plants: Colocasia Esculenta. Retrieved April 21, 2018, from. http://tropical.theferns.info/viewtropical.php?id=colocasia+esculenta.

Fox, J., Weisberg, S., 2012. Robust Regression. Retrieved from. https://www.bauer.uh.edu/rsusmel/phd/fw-robustreg.pdf.

Gaffney, J.J., Baird, C.D., 1977. Forced-air cooling of bell peppers in bulk. Trans. ASAE 20 (6), 1174–1179.

Giavarina, D., 2015. Understanding Bland altman analysis. Biochem. Med. 25 (2), 141–151.

Giner, S.A., Irigoyen, R.M.T., Cicuttín, S., Fiorentini, C., 2010. The variable nature of Biot numbers in food drying. J. Food Eng. 101 (2), 214–222.

Glavina, M., Di Scala, K., del Valle, C., 2007. Effect of dimensions on the cooling rate of whole potatoes applying transfer functions. LWT - Food Sci. Technol. (Lebensmittel-Wissenschaft -Technol.) 40 (10), 1694–1697.

Golbraikh, A., Tropsha, A., 2002. Beware of q2. J. Mol. Graph. Model. 20 (4), 269–276.

Haagenson, D.M., Klotz, K.L., Campbell, L.G., Khan, M.F.R., 2006. Relationships between root size and postharvest respiration rate. J. Sugar Beet Res. 43 (4), 129–144.

Himeda, M., Yanou, N.N., Nguimbou, R.M., Gaiani, C., Scher, J., Facho, J.B., Mbofung, C.M.F., 2012. Physicochemical, rheological and thermal properties of taro (Colocassia esculenta) starch harvested at different maturity stages. Int. J. Biosci. 2 (3), 14–27. Retrieved from. https://www.cabdirect.org/cabdirect/abstract/20123123914.

Huber, P., 1992. Robust Estimation of a Location Parameter, pp. 492–518.

Huber, P., 2004. Robust Statistics. Wiley. Retrieved from. https://books.google.de/books?id=e62RhdqIdMkC.

Jake, T.M., Tirrell, L., 2020. pyCompare V1.5.1. Retrieved from https://zenodo.org/record/4001461#.Y5sQwnbP1nI.

Jian, Y., Bai, F., Falcoz, Q., Xu, C., Wang, Y., Wang, Z., 2015. Thermal analysis and design of solid energy storage systems using a modified lumped capacitance method. Appl. Therm. Eng. 75, 213–223.

Korese, J.K., Sturm, B., Román, F., Hensel, O., 2017. Simulation of transient heat transfer during cooling and heating of whole sweet potato (Ipomoea batatas (L.) Lam.) roots under forced-air conditions. Appl. Therm. Eng. 111, 1171–1178 (L).

Krokida, M.K., Zogzas, N.P., Maroulis, Z.B., 2002. Heat transfer coefficient in food processing: compilation of literature data. Int. J. Food Prop. 5 (2), 435–450.

Kumar, R., Kumar, A., Murthy, U.N., 2008. Heat transfer during forced air precooling of perishable food products. Biosyst. Eng. 99 (2), 228–233.

Kumar, V., Sharma, H.K., Singh, K., 2017. Effect of precooking on drying kinetics of taro (Colocasia esculenta) slices and quality of its flours. Food Biosci. 20, 178–186.

Kundu, P., Cohen, I., Dowling, D. (Eds.), 2012. Compressible Flow. In Fluid Mechanics, fifth ed. Elsevier, pp. 729–778.

Levene, H., 1960. Robust tests for equality of variances. In: Olkin, I., Hotelling, H. (Eds.), Contributions to Probability and Statistics: Essays in Honor of Harold Hotelling. Stanford University Press, pp. 278–292.

Lewu, M.N., Adebola, P.O., Afolayan, A.J., 2010. Comparative assessment of the nutritional value of commercially available cocoyam and potato tubers in South Africa. J. Food Qual. 33 (4), 461–476.

Lin, L., 1989. A concordance correlation coefficient to evaluate reproducibility. Biometrics 45 (1), 255.

Lin, L., Hedayat, A.S., Sinha, B., Yang, M., 2002. Statistical methods in assessing agreement. J. Am. Stat. Assoc. 97 (457), 257–270.

M Alcantara, R., 2013. The nutritional value and phytochemical components of taro [colocasia esculenta (L.) Schott] powder and its selected processed foods. J. Nutr. Food Sci. 3 (3).

Marcotte, M., Chen, C.R., Grabowski, S., Ramaswamy, H.S., Piette, J.-P.G., 2008. Modelling of cooking-cooling processes for meat and poultry products. Int. J. Food Sci. Technol. 43 (4), 673–684.

Modi, A.T., 2007. Effect of indigenous storage method on performance of taro [ Colocasia esculenta (L.) Schott] under field conditions in a warm subtropical area. S. Afr. J. Plant Soil 24 (4), 214–219.

Morley, S.K., Brito, T.V., Welling, D.T., 2018. Measures of model performance based on the log accuracy ratio. Space Weather 16 (1), 69–88.

Ndisya, J., Gitau, A., Roman, F., Mbuge, D., Kulig, B., Sturm, B., Hensel, O., 2021. Convective cooling of purple-speckled cocoyam (colocasia esculenta (L.) Schott): influence of air velocity, tuber size and orientation on cooling behaviour. In: *5th*

*International Conference of the International Commission of Agricultural and Biosystems Engineering (CIGR)*. Québec City. Canada.
Ndisya, J., Mbuge, D., Kulig, B., Gitau, A., Hensel, O., Sturm, B., 2020. Hot air drying of purple-speckled Cocoyam (Colocasia esculenta (L.) Schott) slices: optimisation of drying conditions for improved product quality and energy savings. Therm. Sci. Eng. Prog. 18, 100557.
Opara, L., 1999. CIGR handbook of agricultural engineering, volume IV agro processing engineering, chapter 2 root crops, Part 2.6 storage of edible aroids. In: CIGR Handbook of Agricultural Engineering Volume IV Agro-Processing Engineering. American Society of Agricultural and Biological Engineers, St. Joseph, MI.
Opara, L., 2003. Edible Aroids: Post-Harvest Operation. Palmerston North.
Opata, P.I., Ogbonna, P.E., 2015. Storage profitability and effectiveness of storage methods in yield loss reduction in cocoyam in southeast Nigeria. Afr. J. Agric. Res. 10 (49), 4496–4504.
Pedregosa, F., Varoquaux, G., Gramfort, A., Michel, V., Thirion, B., Grisel, O., et al., 2011. Scikit-learn: machine learning in Python. J. Mach. Learn. Res. 12 (Oct), 2825–2830.
Pham, Q., 2002. Calculation of processing time and heat load during food refrigeration. In: Food for Thought - Cool AIRAH Conference. International Institute of Refrigeration, Sydney, Australia. Retrieved from. https://iifir.org/en/fridoc/119462.
Phongikaroon, S., Calabrese, R.V., 2005. Effect of internal and external resistances on the swelling of droplets. AIChE J. 51 (2), 379–391.
Ranmode, V., Singh, M., Bhattacharya, J., 2019. Analytical formulation of effective heat transfer coefficient and extension of lumped capacitance method to simplify the analysis of packed bed storage systems. Sol. Energy 183, 606–618.
Rohsenow, W., Hartnett, J., Cho, Y., 1998. Handbook of Heat Transfer, third ed. McGraw-Hill, New York, USA.
Romdhana, H., Lambert, C., Goujot, D., Courtois, F., 2016. Model reduction technique for faster simulation of drying of spherical solid foods. J. Food Eng. 170, 125–135.
Shrestha, L., Crichton, S.O.J., Kulig, B., Kiesel, B., Hensel, O., Sturm, B., 2020. Comparative analysis of methods and model prediction performance evaluation for continuous online non-invasive quality assessment during drying of apples from two cultivars. Therm. Sci. Eng. Prog. 18, 100461.
Mean Absolute percentage error (MAPE). In: Swamidass, P.M. (Ed.), 2000. Encyclopedia of Production and Manufacturing Management. Springer US, Boston, MA, p. 462.
Tegenaw, P.D., Gebrehiwot, M.G., Vanierschot, M., 2019. On the comparison between computational fluid dynamics (CFD) and lumped capacitance modeling for the simulation of transient heat transfer in solar dryers. Sol. Energy 184, 417–425.
Thompson, A., 2003. Fruits and Vegetables: Harvesting, Handling and Storage. Retrieved from, second ed. Blackwell Publishing Ltd, Oxford, UK. _handling_and_storage,_2nd_ed.pdf. https://ubblab.weebly.com/uploads/4/7/4/6/47469791/fruit_&_vegetables_harvesting.
Ungerer, J.P.J., Pretorius, C.J., 2017. Method comparison – a practical approach based on error identification. Clin. Chem. Lab. Med. 56 (1), 1–4.
van der Sman, R.G.M., 2003. Simple model for estimating heat and mass transfer in regular-shaped foods. J. Food Eng. 60 (4), 383–390.
van Gogh, B., Boerrigter, H., Noordam, M., Ruben, R., Timmermans, T., 2017. Post-Harvest Loss Reduction: a Value Chain Perspective on the Role of post-harvest Management in Attaining Economically and Environmentally Sustainable Food Chains. Wageningen Food & Biobased Research.
Virtanen, P., Gommers, R., Oliphant, T.E., Haberland, M., Reddy, T., Cournapeau, D., et al., 2020. SciPy 1.0: Fundamental Algorithms for Scientific Computing in Python. Nature Methods, 1. 0.
Wang, J., Higa, S., 1983. Taro, a Review of Colocasia Esculenta and its Potentials. University of Hawaii Press, Honolulu, Hawaii. Retrieved from. https://scholarspace.manoa.hawaii.edu/bitstream/10125/23024/%234_Wang.pdf.
Wang, S., Tang, J., Cavalieri, R.P., 2001. Modeling fruit internal heating rates for hot air and hot water treatments. Postharvest Biol. Technol. 22 (3), 257–270.
Xu, B., Li, P.-W., Chan, C.L., 2012. Extending the validity of lumped capacitance method for large Biot number in thermal storage application. Sol. Energy 86 (6), 1709–1724.
Zdravkovich, M.M., Brand, V.P., Mathew, G., Weston, A., 1989. Flow past short circular cylinders with two free ends. J. Fluid Mech. 203, 557–575.
Zhang, Z., Wei, Q., Liu, C., Li, D., Liu, C., Jiang, N., 2017. Comparison of four pretreatments on the drying behavior and quality of taro (Colocasia esculenta L. Schott) slices during intermittent microwave vacuum-assisted drying. Dry. Technol. 35 (11), 1347–1357.
Zou, Q., Opara, L.U., McKibbin, R., 2006a. A CFD modeling system for airflow and heat transfer in ventilated packaging for fresh foods: I. Initial analysis and development of mathematical models. J. Food Eng. 77 (4), 1037–1047.
Zou, Q., Opara, L.U., McKibbin, R., 2006b. A CFD modeling system for airflow and heat transfer in ventilated packaging for fresh foods:II. Computational solution, software development, and model testing. J. Food Eng. 77 (4), 1048–1058.